

## Quantitative model of reactive metal-semiconductor interface growth using high-resolution photoemission results

R. A. Butera,\* M. del Giudice, and J. H. Weaver

*Department of Chemical Engineering and Materials Science, University of Minnesota, Minneapolis, Minnesota 55455*

(Received 15 July 1985; revised manuscript received 22 November 1985)

High-resolution core-level photoemission studies of the reactive metal-semiconductor interfaces V/Ge(111), Ce/Si(111), and Ce/Ge(111) show that intermixing leads to unique chemical environments or species having well-defined chemical shifts. Decomposition of the coverage-dependent core-level emission shows the growth and attenuation of each of these species. We present a model which quantitatively describes the evolution of the interface. We show that two-phase growth can be described by the lever rule, such that bulk thermodynamic partitioning applies to interfaces having thicknesses of tens of angstroms or less. From the modeling, we extract values for the onset coverage of each phase, the composition of each phase, and the coverage at which each ceases to form. These interface phase diagrams indicate that the first phase is not consumed when subsequent phases form. Application and refinement of these analysis techniques should lead to predictive abilities for junction formation and interface stability.

### INTRODUCTION

The physical and chemical properties of metal-semiconductor interfaces have been the subject of numerous experimental and theoretical studies for decades.<sup>1,2</sup> Many techniques have been used to try to understand the complex reaction chemistry and intermixing of junctions. Issues of great importance include the reactivity of the interface,<sup>3-7</sup> its morphology,<sup>8-10</sup> its spatial extent, its stability, and its electrical behavior (Schottky barrier).<sup>11</sup> Although there has been enormous progress in qualitatively understanding interface properties, we are still far from the kind of quantitative understanding that allows predictive capabilities.

It is the purpose of this paper to show that high-resolution synchrotron radiation photoemission studies can be used to extract the information needed for *quantitative* modeling of the interfacial zone on the scale of tens of angstroms or less. We will show that a relatively simple, continuum-based model can provide an interface phase diagram for such constrained systems. In the process, we will also show that bulk thermodynamics can be applied to the intermixed phases even when they are very thin.

The major conclusions of this paper are the following.

(1) After intermixing occurs at metal-semiconductor interfaces, well-defined species form. The evidence for this is the decomposition of experimental results for V/Ge,<sup>12</sup> Ce/Si,<sup>13</sup> Ce/Ge,<sup>14</sup> Ce/GaAs,<sup>15</sup> and others.<sup>16</sup>

(2) The simultaneous growth of more than one phase is possible, limited by the availability of atomic components and partitioned according to the lever rule of thermodynamics.<sup>17</sup>

(3) The phase which forms at the interface persists during room-temperature interface growth and is not consumed by formation of subsequent phases, although changes in temperature do modify the equilibrium conditions.<sup>18</sup>

(4) The photoelectron scattering properties of each species must be included when attenuation curves are used for modeling.<sup>19</sup>

(5) The final species of a reaction, which has often been associated with surface-segregated semiconductor atoms,<sup>20</sup> is a metal-rich phase.

(6) Metal accumulation and covering up occurs when there are insufficient semiconductor atoms to sustain reactions.

Based on these conclusions, we feel that interface modeling can ultimately become quantitative.<sup>21</sup> A particularly important application of quantitative descriptions is the modeling of the Schottky barrier formation, i.e., its dependence on morphology and the properties of the reacted interface. Likewise, once an interface phase diagram can be created, it becomes possible to predict the stability of the junction. Although we feel that this paper represents a major step, it is only the first step. Future work must push for even higher photoemission resolution and must explore the effects of temperature on reaction kinetics.<sup>18</sup>

In the following we briefly review the experimental techniques and results, discuss the use of photoemission attenuation curves to extract quantitative information, present the mathematical formalism, and apply it to the representative systems V/Ge(111),<sup>12</sup> Ce/Si(111),<sup>7,13</sup> and Ce/Ge(111).<sup>14</sup> These systems were chosen because each is highly reactive, because the chemical shifts for the reaction products are large, and because the core levels were readily accessible using synchrotron radiation. The technique, however, is applicable to other systems, including compound semiconductors, and efforts are presently underway to describe these more complex interfaces. The choice of the cleavage surface for examination was based on convenience, and similar results should be expected for other surfaces when account is taken of differences related to the onset of reaction.

## EXPERIMENTAL TECHNIQUES AND RESULTS

Synchrotron radiation photoemission experiments were conducted at the University of Wisconsin—Madison Synchrotron Radiation Center at Stoughton using radiation from the Tantalus storage ring. The white radiation was dispersed using the Grasshopper Mark II and the 3-m toroidal grating monochromators. Si and Ge crystals oriented along the (111) direction were cut, notched, etched, mounted on sample holders, and introduced into

the photoemission spectrometer. Surfaces for examination were prepared *in situ* by cleaving. The quality of each cleave was assessed visually and was then characterized by photoemission prior to the deposition of metal overlayers. Vanadium and cerium were evaporated from resistively heated sources which had been extensively out-gassed prior to the measurements to ensure the absence of contamination. Evaporation rates were maintained at less than 1 Å per minute and were measured using a quartz-crystal thickness monitor. The source to sample distance

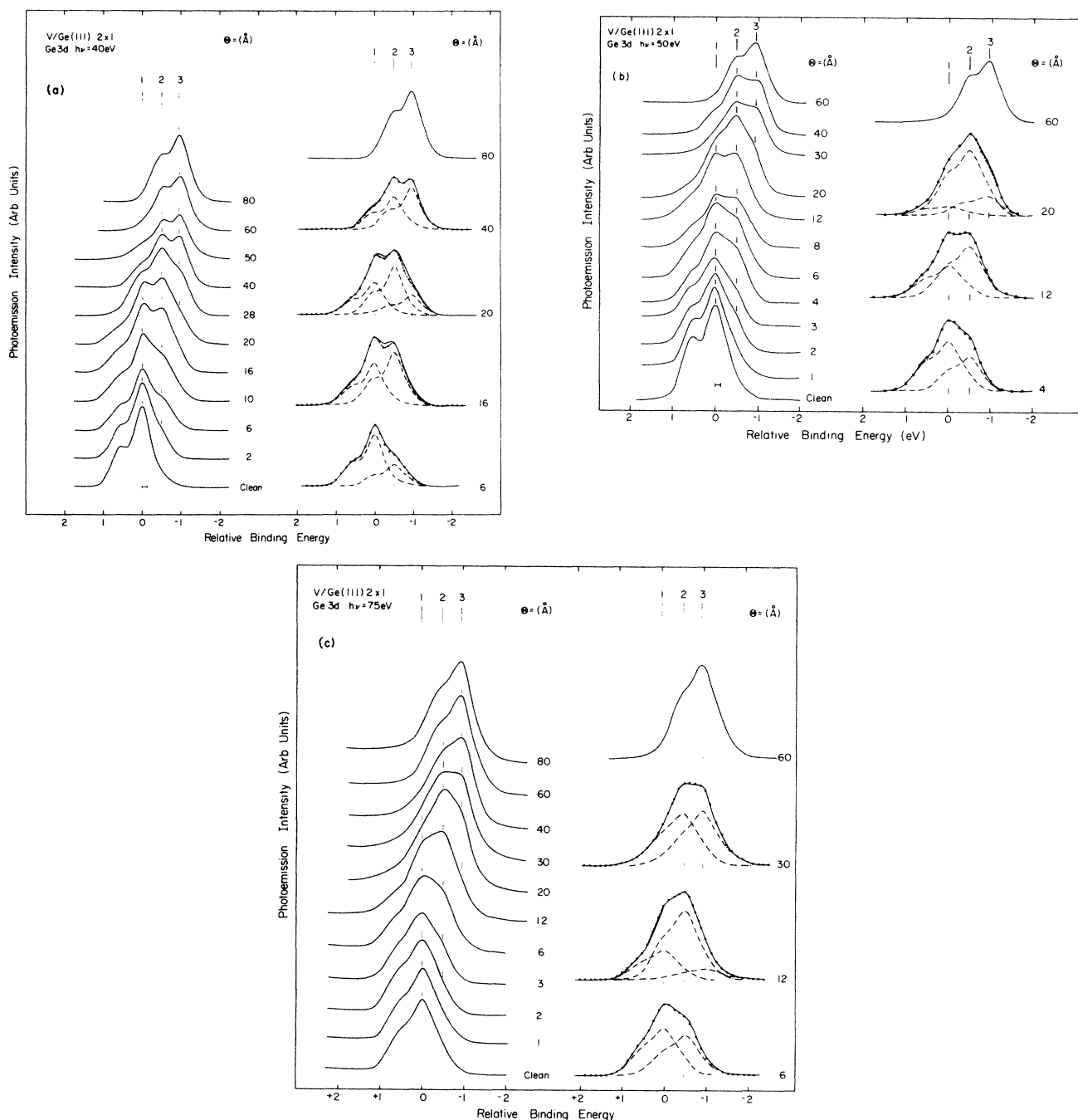


FIG. 1. Ge 3d core-level energy distribution curves (EDC's) showing interface development as a function of coverage,  $\Theta$ , for photon energies of 40, 50, and 75 eV. These spectra have been corrected for initial band bending changes and the backgrounds have been subtracted. Each set of EDC's shows the growth of two reacted components, as indicated, with the results at highest photon energy being the most surface sensitive. Decompositions of the EDC's at representative coverages are shown on the right.

was  $\sim 30$  cm. During deposition, the pressure in the chamber never exceeded  $2 \times 10^{-10}$  Torr. The operating pressure was  $(3-5) \times 10^{-11}$  Torr. The results presented here were obtained with the substrate at room temperature. They are representative of a large number of cleaves and depositions, and the scatter in the experimental points is indicative of the quality of the results.

In Figs. 1–3 we show high-resolution photoemission results for the Ge 3*d* or Si 2*p* cores at the V/Ge interface (Fig. 1), the Ce/Si interface (Fig. 2), and the Ce/Ge interface (Fig. 3). For V/Ge, we show energy distribution curves (EDC's) taken at  $h\nu = 40, 50,$  and  $75$  eV to demonstrate the variation in surface sensitivity. These EDC's have been scaled for visual clarity to be of approximately the same height, and the backgrounds have been subtracted. Corrections for changes in band bending have also been made (125 meV for V/Ge, 200 meV for Ce/Si, and 230 meV for Ce/Ge). Line shape decompositions for representative EDC's are shown on the right of Figs. 1–3. As discussed elsewhere,<sup>22</sup> line shapes derived from the clean surface (with the surface component removed<sup>23</sup>) were used to build subsequent spectra. The binding energy for each species was held fixed throughout the fitting procedures and only the relative intensities of the components were allowed to vary. The decompositions of Figs. 1–3 then indicate that the regions under investigation are composed of distinct chemical environments or phases. This is a fundamental observation and its validity is demonstrated by the quality of the fits and their self-consistency for all coverages. For V/Ge and Ce/Si, we

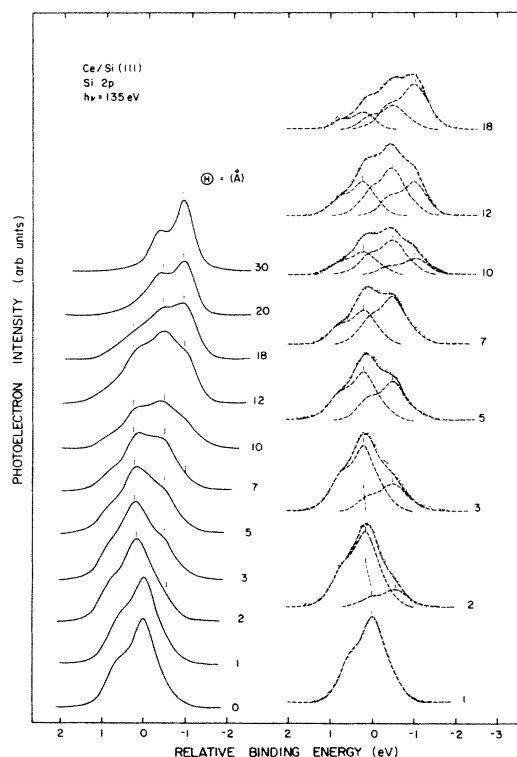


FIG. 2. Si 2*p* core-level EDC's for the Ce/Si(111) interface analogous to those of Fig. 1.

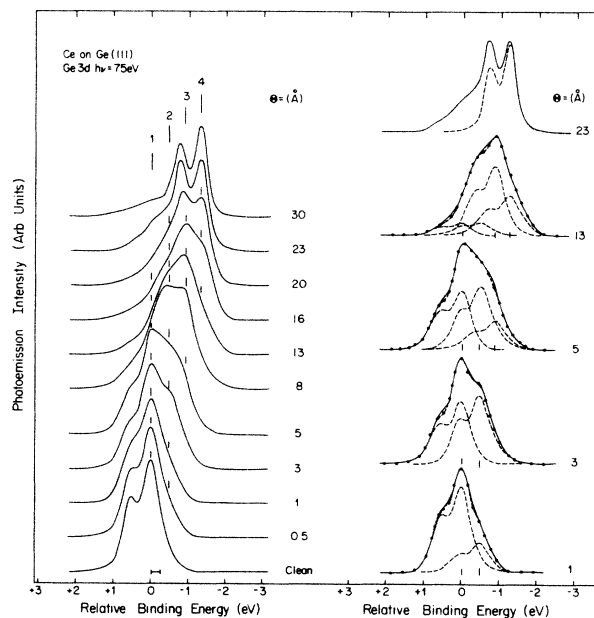


FIG. 3. Ge 3*d* core-level EDC's for the Ce/Ge(111) interface analogous to those of Fig. 1.

needed only two reaction products; for Ce/Ge, we needed a third.

In the decomposition procedures, the number of phases or bonding configurations and their chemical shifts were determined directly from the evolving core-level spectra. The reliability of the decomposition method lies in the fact that we were able to fit not just one spectrum but each EDC in the set. At the same time, it could be argued that core-level shifts might not be large and that two different phases could overlap and contribute to the EDC's and the attenuation-growth curves. We have observed just this effect for Ce/GaAs,<sup>15</sup> but it was straightforward to detect the overlap from the attenuation curves. Finally, in the decompositions, we found very small changes in line shape on going from the substrate to the initial and final reaction products (variations in branching ratio, slight broadening due to inhomogeneities, different types of backgrounds, etc.). Errors in assessing such changes would have negligible effects on our attenuation curves because the fitting errors were within the scatter of the experimental points.

In Figs. 4–6 we show the normalized attenuation curves,  $\ln[I(\Theta)/I(0)]$ , for the three interfaces under examination. The uppermost line in each panel corresponds to the normalized total integrated intensity of all Ge- or Si-related core emission. The other points correspond to the component-specific attenuation extracted by considering each of the species of Figs. 1–3 individually. The dashed lines represent the fits based on our model, to be discussed in a later section.

The results of the decomposition make it possible to identify several interface regions. The first corresponds to the initiation of reaction when the first species grows and becomes larger than the rapidly decaying substrate contribution. The next corresponds to the region where the to-

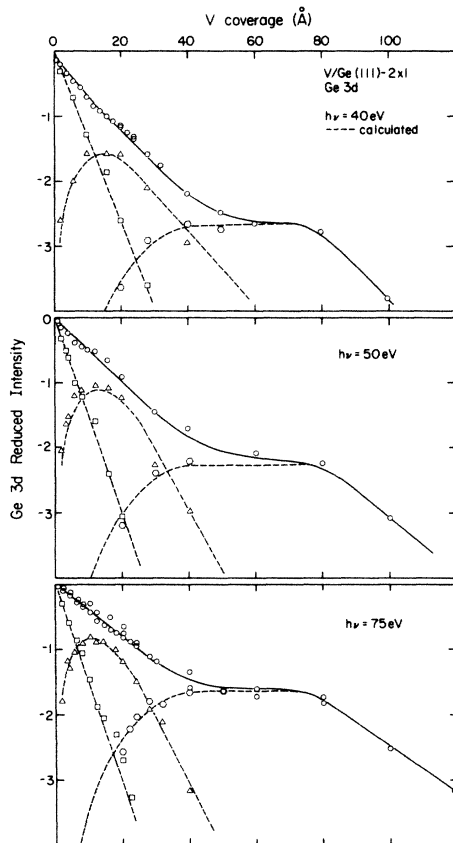


FIG. 4. Ge 3d growth-attenuation curves for the V/Ge(111) interface showing normalized intensities of the total core emission as a function of coverage,  $\ln[I(\Theta)/I(0)]$ , for different photoelectron escape depths. The total intensities are given by solid lines connecting open circles. The component-specific intensities were obtained from the decompositions of Fig. 1 (open three-, four-, and six-sided symbols). The dashed curves are the result of the fits discussed in the text. In each case, the substrate emission can be seen to diminish rapidly, the first reacted component grows to a maximum near 15 Å, the second reacted component dominates above about 35 Å, and rapid overall attenuation is observed after 80 Å of V deposition.

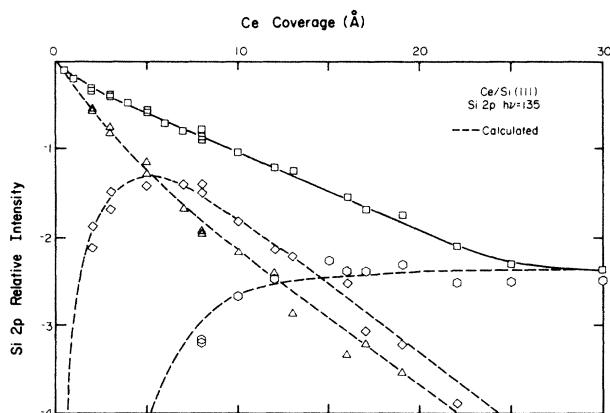


FIG. 5. Si 2p growth-attenuation curves at  $h\nu=135$  eV for the Ce/Si(111) interface analogous to those of Fig. 4.

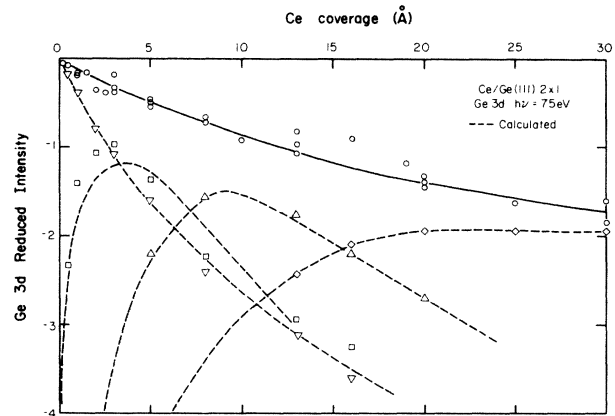


FIG. 6. Ge 3d growth-attenuation curves analogous to those of Fig. 4. In the three-phase region (2–8 Å) the approximations used do not allow as good a fit as for the two-phase regions, as discussed in the text, but the fit is still reasonable.

tal attenuation curve exhibits a plateau. The final region corresponds to the covering up of the reacted region by the metal overlayer. This behavior appears to be generic, although the details vary with overlayer-substrate pairs. Indeed, this variation is significant for understanding the systematics of formation.

Figures 1–6 summarize the experimental results necessary for modeling. We shall return to them after the discussion of the interpretation of attenuation curves and the discussion of the reaction chemistry expected at these interfaces.

#### PHOTON ENERGY VARIATIONS AND MEASURED ATTENUATION CURVES

In the following we assume that the photoelectron intensity  $I_i(\Theta)$  associated with the  $i$ th species when metal atoms corresponding to a coverage  $\Theta$  have been deposited onto a semiconductor which has atomic density  $C_i$  can be written

$$I_i(\Theta) = \sigma_i(E) C_i T(E_{\text{kin},i}) I(E) \int e^{-\mu_i x} e^{-x/\lambda_i} dx, \quad (1)$$

where  $\sigma_i$  is the photoabsorption cross section for the semiconductor atoms in the  $i$ th species,  $T(E_{\text{kin},i})$  takes into account the transmission properties of the analyzer at a kinetic energy  $E_{\text{kin},i}$ ,  $I(E)$  is the photon beam intensity, the limits of integration correspond to the spatial extent of the species under consideration,  $\mu_i(E)$  is the photon absorption coefficient, and  $\lambda_i(E)$  is the photoelectron escape depth.  $I(0)$  corresponds to the emission from the semiconductor atoms for the clean surface. Reflection at the surface has been neglected.

For a multilayer system where the  $i$ th phase is built with a thickness  $\Theta$  over the substrate, Eq. (1) becomes

$$I_i = \sigma_i(E) C_i T(E_{\text{kin},i}) \frac{\lambda_i}{1 + \mu_i \lambda_i} \times I(E) \left[ 1 - \exp \left[ -\frac{\Theta}{\lambda_i} (1 + \mu_i \lambda_i) \right] \right]. \quad (2)$$

Since the photon penetration depth is several orders of magnitude larger than the photoelectron mean free path, we can write  $(1 + \mu_i \lambda_i) = 1$ , giving

$$I_i(\Theta) = \sigma_i(E) C_i T(E_{\text{kin},i}) \lambda_i I(E) \left[ 1 - \exp \left[ -\frac{\Theta}{\lambda_i} \right] \right]. \quad (3)$$

Analogously, we can write for the substrate

$$I_s(\Theta) = \sigma_0(E) C_0 T(E_{\text{kin},0}) \lambda_0 I(E) \exp \left[ -\frac{\Theta}{\lambda_0} \right]. \quad (4)$$

We can then form the ratio of Eqs. (3) and (4) to get the measured quantity

$$\frac{I_i(\Theta)}{I_s(0)} = \frac{\sigma_i(E) C_i \lambda_i(E) T(E_{\text{kin},i}) \left[ 1 - \exp \left[ -\frac{\Theta}{\lambda_i} \right] \right]}{\sigma_0(E) \lambda_0(E) T(E_{\text{kin},0})}, \quad (5)$$

where we have normalized to the clean substrate core-level intensity ( $\Theta=0$ ) and taken  $C_0$  to be unity. In this way  $C_i$  is actually the ratio of the atomic densities  $C_i/C_0$  and has the dimension of an atomic fraction. In Eq. (5) reflection of electrons at the interface is neglected.

Equation (5) can be simplified as follows. First, the difference in kinetic energy between photoelectrons from the unreacted semiconductor atom and from the  $i$ th reacted species is  $\lesssim 1.2$  eV. Since the transmission function for the electron energy analyzer is a slowly varying function of kinetic energy, we let  $T(E_{\text{kin},i}) = T(E_{\text{kin},0})$ . Second, the ratio of  $\sigma_i/\sigma_0$  can be approximated as unity. Far from threshold, we might expect that this approximation would be quite good since the photoelectron transition occurs between the atomic core level and the continuum. Close to threshold, the influence of the environment would be larger because the final states are modified in bonding.<sup>24</sup> We do note, however, that good fits to the evolving core-level emission are obtained by using the spin-orbit branching ratio obtained from the unreacted semiconductor. With these approximations, we can write

$$I_i(\Theta)/I_s(0) = C_i (\lambda_i/\lambda_0) [1 - \exp(-\Theta/\lambda_i)]. \quad (6)$$

Equation (6) is fundamental for interpreting the results of attenuation curves taken at a variety of photon energies

and for quantitative evaluations of atomic concentrations in the reacted region. Many studies, including our own, have normalized the measured intensity  $I_i(\Theta)$  to that of the clean substrate  $I_s(0)$  and have assumed that the kinetic energy dependence of the photoelectron escape depth is independent of the material in question.<sup>19</sup> In Fig. 4 we show experimental results for V/Ge which demonstrate that the apparent total Ge content appears to be greatest when the surface sensitivity is largest. This observation has been used to argue for surface segregation of the semiconductor atom—not just for the systems under discussion here but for a good many others<sup>25</sup>—but is chemically not tenable for a system in equilibrium. Reevaluation of the results using Eq. (6) eliminates the need for surface segregation since we find the material-specific scattering parameters  $\lambda_i$ .<sup>26</sup>

To verify that the escape depths do, in fact, vary with the composition of the overlayer, consider a system in which the layer thickness is large enough that the stoichiometry of the region being probed does not change as the photon energy changes. For this case, the intensity of a particular core component is invariant with changes in  $h\nu$ , assuming that the results are normalized to the total number of atoms in the probed region. We can then write Eq. (6) for two different photon energies,  $h\nu$  and  $h\nu'$ , and form the ratio

$$\left[ \frac{I_2}{I_{s0}} \right]_{h\nu} / \left[ \frac{I_2}{I_{s0}} \right]_{h\nu'} = \left[ \frac{\lambda_2}{\lambda_0} \right]_{h\nu} / \left[ \frac{\lambda_2}{\lambda_0} \right]_{h\nu'}. \quad (7)$$

The quantity on the left-hand side of Eq. (7) can be determined experimentally by comparing the intensities of the second component at a coverage  $\Theta$  for two different photon energies using the plateau regions of Fig. 4 for V/Ge. Likewise, we can extract values for  $\lambda_2$  in this region since  $\lambda_2$  is the attenuation of the first reacted phase through the second reacted phase—experimentally, this is the decay slope of phase one. We can repeat this for other pairs of photon energies, getting ratios of  $\lambda_0$  at  $h\nu$  divided by  $\lambda_0$  at  $h\nu'$ . Since  $\lambda_0$  is the escape depth of photoelectrons in crystalline Ge, we can use the Seah-Dench<sup>27</sup> value at any energy  $h\nu$  and we can use the ratios obtained from the interface results to predict  $\lambda_0$  values for all energies  $h\nu'$ . If our modeling is self-consistent, the resulting  $h\nu$  dependence of  $\lambda_0$  must agree with what has been found for pure Ge. As shown in Table I, the results in the fourth and

TABLE I. Experimental values for photoelectron mean free paths (mfp's) at the V/Ge interface. The first column is the photon energy, the second column gives the ratio of the substrate mfp calculated from Eq. (7), the third column gives the experimental results extracted from the growth-attenuation curves for the metal-rich component, the fourth column gives substrate mfp calculated from the second column assuming the substrate mfp to be 5 Å at  $h\nu=75$  eV, the fifth column lists the substrate mfp obtained from the universal curve (Ref. 27).

$h\nu$ (eV)	$\frac{\lambda_0(h\nu)}{\lambda_0(75 \text{ eV})}$	$\lambda_2$ (Å)	$\lambda_0$ (Å)	$\lambda_0$ (Å)
75	1.000	9.8±0.5	5.0	5
50	1.871	10.6±0.5	9.4	10
40	4.198	15.0±0.5	20.9	21

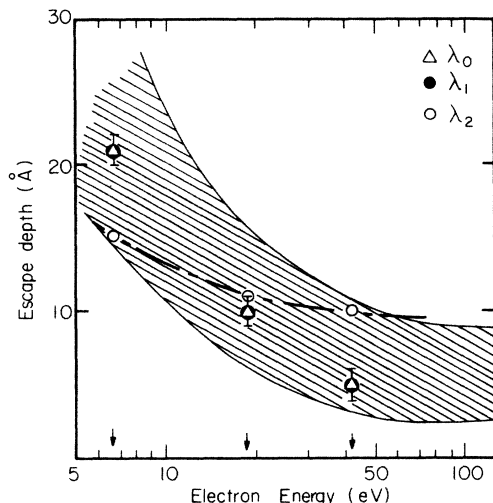


FIG. 7. Variation of the photoelectron escape depth with photon energy. The shaded region corresponds to the envelope of experimental points reported in the literature. The values for  $\lambda_0$  and  $\lambda_1$ , given by triangles and solid circles, correspond to attenuation lengths through the substrate and first reacted phases, as derived from our results. The values for  $\lambda_2$  (open circles) are for the metal-rich final component. The changes in relative magnitudes of these mean free paths explains why the surface sensitive results of Fig. 4 appear to show surface segregation.

fifth columns are in excellent agreement. We therefore conclude that the set of  $\lambda_i$ 's that we determined are self-consistent and the values obtained for photoelectron propagation through the  $i$ th species are valid. From Table I we see that the ratio  $\lambda_i/\lambda_0$  in Eq. (6) is not a constant as has generally always been assumed.<sup>19</sup>

In retrospect, this variation in  $\lambda$  shown in Fig. 7 is intuitively reasonable since the dielectric function of the semiconductor, the silicide or germanide, and the metal are very different. Hence, the plasma frequencies differ significantly (the calculated plasma frequency for Ge is 15.6 eV compared to 22.3 for V). The anomalous  $h\nu$  dependence of the experimental attenuation curves can now be interpreted in terms of the photoemission process itself. It does not justify the assumption of semiconductor atoms floating on the surface of reacted layers.

#### INTERFACE CHEMISTRY AND REACTION PRODUCTS

In the following, we describe interface chemical reactions which can produce well-defined phases. The purpose of this section is to identify the properties of the interface as a function of coverage to produce a phase diagram. The fit of the predicted attenuation curves to experiment will give the values for the parameters (stoichiometry, onset coverage, completion coverage).

When we consider intermixing, we can assume that there will be sufficient disruption of the semiconductor itself to sustain the reactions, coupled with semiconductor atom out diffusion to feed the reactions and provide mass balance. When this is not satisfied, the overlayer con-

verges to the elemental metal. Let  $\Theta_1$  and  $\Theta_1^*$  correspond to the beginning and end points for the first reaction (phase 1) and let  $\Theta_2$  and  $\Theta_2^*$  correspond to the beginning and end points for the second reaction (phase 2). If necessary, a third phase could be introduced, as for Ce/Ge(111). In Fig. 8 we show the resulting generic phase diagram, plotting the range of existence of each phase versus coverage for two phases having different semiconductor contents. Several distinct regions can be identified in the generic two-component phase diagram shown at the top of Fig. 8.

(1) In the region from  $\Theta_1$  to  $\Theta_2$ , a single phase will form because the surface concentration of the semiconductor exclusively supports the reaction ( $xM + yS \rightarrow M_xS_y$ ).

(2) In the range from  $\Theta_2$  to  $\Theta_1^*$ , two phases grow simultaneously, governed by the reactions  $(1-\chi)[xM + yS \rightarrow M_xS_y]$  and  $\chi[uM + wS \rightarrow M_uS_w]$ , where  $\chi$  is given by the lever rule,<sup>28</sup>  $\chi = (\Theta - \Theta_2)/(\Theta_1^* - \Theta_2)$ , and denotes the partitioning of the phases.

(3) For coverages between  $\Theta_1^*$  and  $\Theta_2^*$ , a single phase will again form, governed by  $(uM + wS \rightarrow M_uS_w)$ . In this range there are too few semiconductor atoms to support the formation of the semiconductor-rich phase.

(4) For coverages above  $\Theta_2^*$  metal accumulation starts and there is convergence to the metal.

In the single phase regions of Fig. 8, the growth-attenuation behaviors of the core-level intensities can be described by the standard equations. As the two-phase

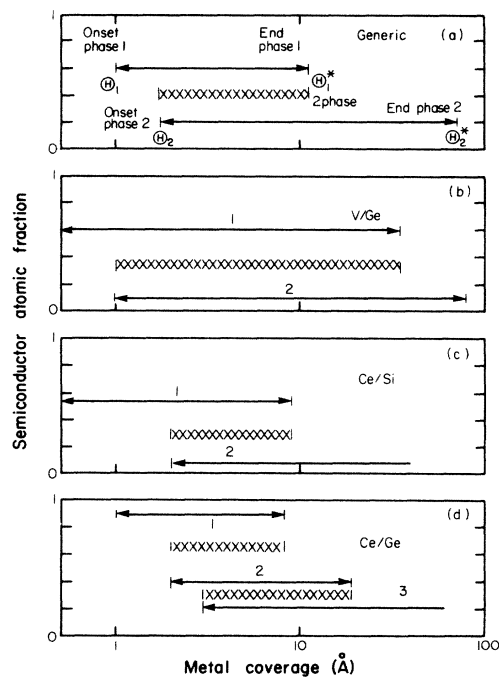


FIG. 8. (a) Proposed phase diagram for an interface where intermixing produces two competing phases.  $\Theta_1$  and  $\Theta_2$  are the onset coverages;  $\Theta_1^*$  and  $\Theta_2^*$  are the completion coverages. The two-phase region exists between  $\Theta_2$  and  $\Theta_1^*$ . The results of our analysis for V/Ge, Ce/Si, and Ce/Ge [(b), (c), and (d)] show how these interfaces are generically similar but how the details vary.

field is entered, however, the new phase appears, coupled with the attenuation of the substrate and the other reacted phase. If growth is at the expense of the first reaction product, then modeling would need to take such consumption into account. However, it is important to note that we have found good agreement with experiment by assuming that the phases which form are stable and non-consuming. We assume a mixture in the two-phase region with partitioning determined from the lever rule of bulk thermodynamics;  $(1-\chi)$  represents the fraction of metal involved in forming the first phase and  $\chi$  represents the second, where  $\chi$  follows from the definition of the two-phase region,

$$\chi = (\Theta - \Theta_2) / (\Theta_1^* - \Theta_2) .$$

As the total overlayer thickness increases, the ratio of first to second reacted phases decreases until, ultimately, the first phase cannot form.

The derivation of the general expressions which describe the intensity of any core component during the kind of evolution represented by Fig. 8 is given in Appendix A. The intensity of phase one, normalized to the substrate intensity for the clean surface, is

$$\frac{I_1(\Theta)}{I_s(0)} = C_1 \left[ \frac{\lambda_1}{\lambda_0} \right] (1 - e^{-\Theta/\lambda_1}) \times [(1-\chi) + \chi e^{-[(\Theta-\Theta_2)/\lambda_2]}] , \quad (8)$$

and that of the second phase is

$$\frac{I_2(\Theta)}{I_s(0)} = \chi C_2 \left[ \frac{\lambda_2}{\lambda_0} \right] (1 - e^{-[(\Theta-\Theta_2)/\lambda_2]}), \quad (9)$$

where the boundary conditions are

$$\Theta_1 < \Theta < \Theta_2, \quad \chi = 0 ,$$

$$\Theta_2 < \Theta < \Theta_1^*, \quad \chi = (\Theta - \Theta_2) / (\Theta_1^* - \Theta_2) ,$$

and

$$\Theta_1^* < \Theta < \Theta_2^*, \quad \chi = 1 .$$

The first bracketed term in Eq. (8) represents the photoemission intensity from a reacted layer of thickness  $\Theta$  with scattering properties included in  $\lambda_1$ . The second term includes photoelectron scattering through the second phase.  $\chi$  and  $1-\chi$  give the amounts of the two phases as a function of  $\Theta$ . In this derivation we have considered only two-phase systems. If three phases coexist, then the formalism must be extended. Unfortunately, the lever rule for three components is no longer linear in  $\chi$  since there are two "levers" which dictate the partition of the phases. We will discuss this case for Ce/Ge, and the way in which it can be solved approximately.

Finally, our model assumes the formation of compounds having definite stoichiometries. It is also possible that solid solutions can be present, as for example at the dilute limit of either very low metal coverages or very high metal coverages. In the case where the solvent is the semiconductor, the solution can vary from pure semicon-

ductor to the saturation value of metal in semiconductor. In such variable-concentration cases, the composition will be controlled by the amount of metal present. In principle, composition variation should be accompanied by continuous shifts in binding energy for the semiconductor core level. In the cases studied to date, however, we have not observed this effect. The results indicate that, within our limits of detectability, the energy of the semiconductor core level associated with the initial reacted phase is constant. Thus, if this phase were, in fact, the solid solution of the metal in the semiconductor, it must correspond to the limiting solubility value, and there must always be sufficient metal locally to form the saturated solid solution. The underlying cause of this is still open to question but may well be related to the bonding characteristics of the constituents involved. The situation for the terminal solution region differs from the metal solution region in that the concentration will be controlled by the semiconductor surface concentration. The rate of attenuation of this final component will then be controlled by both the declining concentration level and the covering effect of the added metal.

To model any interface of the form described above, we must then measure the component-specific core-level intensities with high-resolution photoemission, determine the appropriate material-specific attenuation lengths from the experimental results, and partition the phases through the lever rule. In this procedure, the parameters determined by the fit of one phase must remain invariant when considering the remaining phases—they are *not* independent. Likewise, parameters obtained for results at one-photon energy must not be changed—except the  $\lambda$ 's which are  $h\nu$  dependent. The agreement between the predictions and the experimental results validate the assumptions described above.

Finally, in the equations reported here the thickness of the reacted layer has been expressed as  $\Theta$  in angstroms. This is because the only available measure of the amount of reacted material formed per unit surface area is the amount of metal deposited. Indeed, there is no way to compute the number of monolayers formed for a reactive interface where disruption of the substrate occurs and the density and structure of the interface are unknown. Hence, in comparing our escape depths (in angstroms) to published values for bulk compounds of known character, it should be remembered that our results were obtained by plotting the attenuation curves as a function of metal deposited. Corrections based on the amount of germanide or silicide formed would bring the  $\lambda$ 's into better agreement with the universal curve of Fig. 7 (to be discussed later in this paper).

## APPLICATION OF THE MODEL

### V/Ge(111)

In Fig. 1 we show EDC's for the V/Ge interface taken at photon energies of 40, 50, and 75 eV, and in Fig. 4 we show corresponding attenuation curves. Based on the analysis described above, we propose the phase diagram for this system given in Fig. 7(b), as derived with the fitting parameters listed in Table II, and we can now quanti-

TABLE II. Summary of the fitting parameters for V/Ge(111).  $\Theta_1$  and  $\Theta_2$  are the critical coverages at which phase 1 and phase 2 form, respectively.  $\Theta_1^*$  and  $\Theta_2^*$  are the points where each species stops.  $\chi_{\text{Ge}}$  is the atomic fraction and represents the result of the fit. As shown, it is consistent for the three different energies.

$h\nu$ (eV)	$\lambda_0$ (Å)	$\lambda_1$	$\lambda_2$	$\Theta_1$	$\Theta_2$	$\Theta_1^*$	$\Theta_2^*$	$(\chi_{\text{Ge}})_1$	$(\chi_{\text{Ge}})_2$
75	5	5	9.8	0±1	1±1	34	80	0.60	0.10
50	10	10	10.6	0±1	1±1	34	80	0.60	0.10
40	21	21	15	0±1	1±1	34	80	0.60	0.10

tatively describe the evolution of the V/Ge(111) interface. The first reaction product induced by V deposition onto Ge(111) is characterized by a Ge atomic fraction of  $0.60 \pm 0.05$  which corresponds to the formula  $\text{V}_2\text{Ge}_3$ . Phase two starts to form after a coverage of  $1 \pm 1$  Å, and it grows through the coverage which corresponds to the cessation of phase one growth ( $34 \pm 1$  Å). It is not until  $\sim 80$  Å of coverage that pure vanadium metal starts to accumulate on the surface because there is insufficient Ge to sustain the metal-rich or phase-two reaction.

It is important to recognize that the lowest coverage at which we can clearly detect the second reacted phase from our EDC's is  $\sim 18$  Å. In contrast, the fit of Fig. 4 to the experimental results indicates that the reaction has started at  $\sim 1$  Å. This is an important outcome of quantitative modeling and is indeed one of the ultimate goals: By modeling we can extrapolate the behavior of the interface to the dilute limits. The reason for the relatively late detection of the second phase is straightforward—the amount of Ge in this phase is small compared to crystalline Ge or the earlier  $\text{V}_2\text{Ge}_3$  phase, and the detection of a phase of low concentration in a dilute matrix is difficult.

In a recent paper<sup>12</sup> we evaluated the ultralow coverage region before reaction set in for V/Ge(111) and showed that vanadium deposition leads to the formation of three-dimensional islands or clusters. Detailed line-shape analysis showed that it was not until a critical coverage of  $\sim 2$  Å that there was clear evidence for a reacted component in the Ge core emission. In this prereacted stage of interface formation we should not expect that the present continuum model would be as reliable as the direct experimental results. At the same time, in both instances where clusters form at ultralow coverages (V/Ge and Ce/Si), we note that the model predicts reaction at  $\sim 1$  Å, which is not inconsistent with the direct results.

It should be noted that the substrate fit has been obtained by taking the difference between the experimental total attenuation curve and the sum of the component fits obtained using our model. The results of this process are in good agreement with the values obtained from the core decompositions. We have not as yet been able to explain or model the lack of  $h\nu$  dependence of the slope of the substrate attenuation. Possible interpretations may require the introduction of morphological changes at the interface during substrate disruption, involving such effects as cluster formation and/or indiffusion of metal atoms. We were able, in fact, to fit the results for the substrate for one-photon energy, but no consistency was found at different photon energies using the values reported in

Table I for the escape depths. More accurate and detailed investigations at low coverages are needed to shed light on this problem, and studies in this direction are in progress. Another consideration concerns the attenuation of the signal by the metal overlayer ( $\Theta > 80$ ). We did not attempt a fit of this region because of the magnitude of the signal and the error bars on each point.

#### Sequential versus simultaneous growth.

It is difficult to prove whether sequential reactions occur at the interface where the first phase is used to form the second phase. Our results show that the best agreement with the experimental data is obtained by assuming no conversion between the two reacted phases. Some insight into the problems related to this issue can be gained by considering the following example.

Let us assume that the first phase in its development reaches a point  $\Theta_c$  in the value of metal coverage where it stops growing and the second phase begins to form, consuming the first one. In this way, using the same notation as above, we can write for  $\Theta_1 < \Theta_c \leq \Theta_2$

$$\frac{I_1}{I_0} = \left[ \frac{x+y}{x} \right] \frac{\lambda_1}{\lambda_0} \left[ 1 - \exp \left[ - \frac{\left[ \frac{x+y}{x} \right] (\Theta - \Theta_1)}{\lambda_1} \right] \right],$$

and for  $\Theta_2 \leq \Theta_c \leq \Theta_2$

$$\frac{I_1}{I_0} = \left[ \frac{x+y}{x} \right] \frac{\lambda_1}{\lambda_0} (1 - e^{-T_1/\lambda_1}),$$

where

$$T_1 = \left[ \frac{x+y}{x} \right] (\Theta_c - \Theta_1) - \left[ \frac{u}{w} \right] (\Theta - \Theta_2)$$

is the thickness of the first reacted phase and

$$T_2 = \left[ \frac{u+w}{w} \right] (\Theta - \Theta_2)$$

is the thickness of the second one. If, for example, we assume a sequential reaction of the form  $\text{V} + 2\text{G} \rightarrow \text{VGe}_2$  followed by  $17\text{V} + \text{VGe}_2 \rightarrow 2\text{V}_9\text{Ge}$ , then we have for the reaction coefficients the values  $x=1$ ,  $y=2$ ,  $w=17$ ,  $u=1$ .

In the top panel of Fig. 9 we report the results at  $h\nu=40$  eV for two values of  $\lambda$  for both reacted phases ( $\lambda_1=10$  and  $\lambda_1=21$  for the lower and the upper dashed

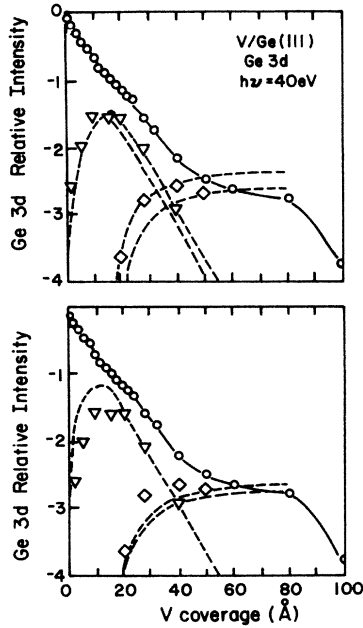


FIG. 9. Ge 3d attenuation curves for the V/Ge(111) interface at  $h\nu=40$  eV. The attenuation of the substrate has been omitted for simplicity. The top panel shows the best fit of the results assuming growth of the first phase up to 18 Å followed by the growth of the second phase by consumption of the first one. A sharp cusp is observed around 18 Å. The equation and parameters used are discussed in the text. The bottom panel shows the fit of the same results assuming sequential reaction between the first and second phase, removing the constraint that the first phase ceases to grow when the second starts.

curves, respectively). As shown, the fit to the data is not nearly as good as the one obtained in Fig. 4. A sharp cusp is always present at the point where conversion of phase 1 to phase 2 starts ( $\Theta \sim 18$  Å).

If we remove the constraint that the first phase ceases to grow when the second starts, but we still consider a sequential reaction as the mechanism by which the second phase forms, then we can write for the intensity of the first phase

$$\frac{I_1}{I_0} = \left[ \frac{x+y}{x} \right] \frac{\lambda_1}{\lambda_0} \left[ 1 - \exp \left[ - \frac{\left[ \frac{x+y}{x} \right] (\Theta - \Theta_1)}{\lambda_1} \right] \right] \quad \text{for } \Theta_1 < \Theta < \Theta_2,$$

$$\frac{I_1}{I_0} = \left[ \frac{x+y}{x} \right] \frac{\lambda_1}{\lambda_0} (1 - e^{-T_1/\lambda_1}) e^{-T_2/\lambda_2} \quad \text{for } \Theta_2 < \Theta,$$

with

$$T_1 = \left[ \frac{x+y}{x} \right] (\Theta - \Theta_1) - \frac{u}{w} (\Theta - \Theta_2)$$

and

$$T_2 = \left[ \frac{u+w}{w} \right] (\Theta - \Theta_2),$$

where  $T_1$  and  $T_2$  are the thicknesses of the first and the second reacted phases. If we assume a sequential reaction of the kind  $2V + Ge \rightarrow V_2Ge$  followed by  $7V + V_2Ge \rightarrow V_9Ge$ , then we have the results plotted in Fig. 9 (bottom panel). Again, the fit is not satisfactory. Based on this, we believe that interface formation can be described better in terms of the formation of two phases but without interconversion.

In Fig. 10 we report the normal thickness  $T$  of the reacted overlayer versus the thickness of the metal deposited  $\Theta$ . In reality, we might more appropriately define  $T$  as the total amount of material that forms at the interface, in contrast to  $\Theta$  which represents the nominal number of metal atoms deposited. According to our model, each increment of metal evaporated is partitioned in two phases characterized by atomic fractions  $C_1 = y/(x+y)$  and  $C_2 = u/(u+w)$ . The total increment in thickness can be written in the two-phase region ( $\Theta_2 \leq \Theta \leq \Theta_1^*$ ) as

$$\Delta T_{\text{tot}} = \Delta T_1 + \Delta T_2 = (1-\chi) \frac{x+y}{x} \Delta \Theta + \chi \frac{u+w}{w} \Delta \Theta,$$

where  $\Delta T_1$  and  $\Delta T_2$  are the increments for phase 1 and 2, respectively. Then

$$\frac{dT_{\text{tot}}}{d\Theta} = [1-\chi(\Theta)] \frac{x+y}{x} + \chi(\Theta) \frac{u+w}{w}.$$

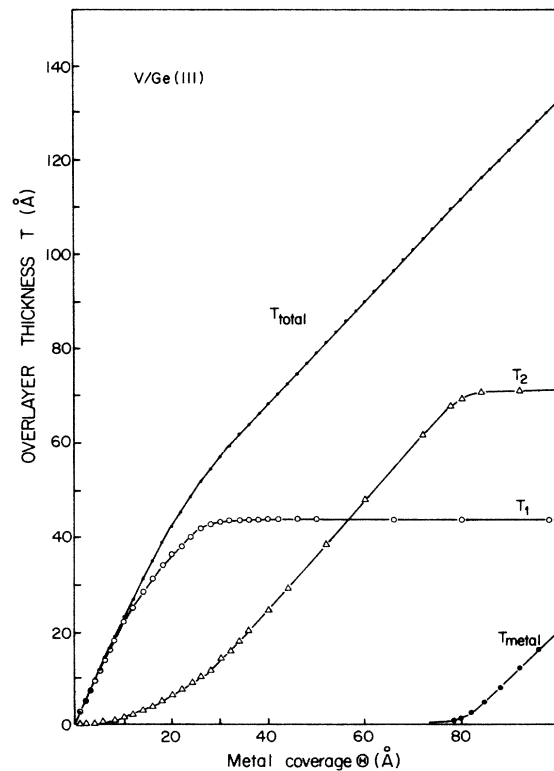


FIG. 10. Overlayer thickness versus metal coverage  $\Theta$ . As shown, the total thickness  $T_{\text{total}}$  does not follow a linear dependence on the  $\Theta$  values. The resulting distortion of the total attenuation curve when plotted against  $\Theta$  must be considered for quantitative interpretation of the results. Also shown are the individual contributions of each single phase.

Integration is straightforward and gives for  $T_{\text{tot}}$  the expression

$$T_{\text{tot}} = \frac{x+y}{x}(\Theta - \Theta_2) - \left[ \frac{x+y}{x} - \frac{u+w}{w} \right] \frac{1}{2} \chi(\Theta)(\Theta - \Theta_2),$$

and for each phase the expressions

$$T_1 = \frac{x+y}{x} \left[ 1 - \frac{1}{2} \chi(\Theta) \right] (\Theta - \Theta_2),$$

$$T_2 = \frac{u+w}{w} \frac{1}{2} \chi(\Theta)(\Theta - \Theta_2).$$

These expressions for  $T_1$  and  $T_2$  are clearly not linear and express the difficulty encountered in obtaining a quantitative model for this kind of interface. As seen in Fig. 10, there is an initial region in which the first phase is practically the only one responsible for the fast growth of the thickness of the film. Subsequently, the second product is increasingly important and the metal concentration ultimately comes into play. During this process,  $T(\Theta)_{\text{total}}$  tends to saturate to a straight line with a slope equal to 1, indicating convergence to a metal overlayer. The slope of the tangent at the origin of the axes is the value of  $(x+y)/x$  (2.5 for  $\text{V}_2\text{Ge}_3$ ). We can then conclude that in our modeling the increment in the thickness of the reacted layer is substantially different from  $\Delta\Theta$  only in the first  $\sim 40$  Å of metal deposition. This expected non-linearity in the growth mode of the interface distorts the attenuation curves, especially in the first 40-Å region. If we correct for this effect, we find that the slope of the attenuation of the substrate corresponds to  $1/e$  decay lengths of 15 Å and 20 Å at 75 eV and 40 eV, respectively, in better agreement with the Seah-Dench values.

We can now plot the atomic concentration of semiconductor atoms as a function of the amount of material in the overlayer. In Fig. 11 we report the results of this analysis. The solid symbols correspond to the total percentage of Ge present in the reacted overlayer, where 100% indicates pure Ge. Results are plotted as a function of  $T$ , the amount of material formed, measured in angstroms. As shown, the Ge concentration in the overlayer drops slowly, starting from the value 0.6 achieved in the first 10 Å, and approaches zero due to the dilution effect generated by the forming metallic overlayer. The signal measured is then proportional to the convolution product

$$I \propto \int \exp(-z/\lambda) \rho(z) dz,$$

where  $\rho(z)$  is the concentration of the semiconductor atoms. This means that the signal is filtered through an exponential window due to the intrinsic properties of the experimental probe. Curves A and B in Fig. 11 show the results of this convolution when we assume that the exponential  $\exp(-z/\lambda)$  can be replaced by a rectangular window described by

$$f(x) = \Theta(x - x_0)\Theta(x_1 - x),$$

where  $\Theta(x)$  is the step function with  $\Theta(x) = 1$  if  $x > 0$  and  $\Theta(x) = 0$  if  $x < 0$ . This is a rough approximation, but results shed some light on the origin of the plateau in the at-

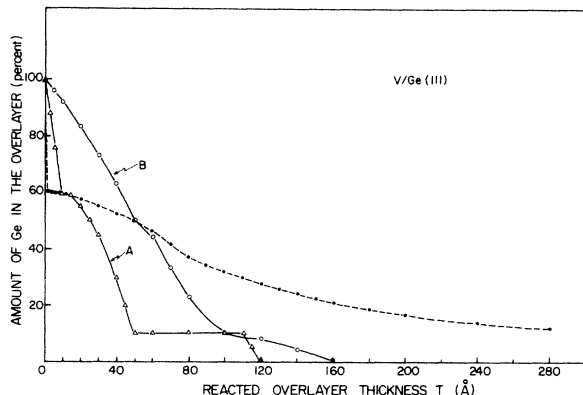


FIG. 11. Percent of Ge dissolved in the reacted overlayer versus its nominal thickness  $T$  in Å (black symbols). Curves A and B refer to the attenuation curve that would be observed assuming for the probe transmission function a window of 5 Å and 20 Å, respectively. This shows that the plateau range in the data reported in Figs. 4 and 5 can be emphasized by the interplay of the Ge density and the experimental probe itself.

tenuation curves. Indeed, curves A ( $x_0=0$ ,  $x_1=10$  Å) and B ( $x_0=x$ ,  $x_1=50$  Å) show that in both cases the total concentration seen with our probe drops continuously from 100% and exhibits a typical plateau that is more or less extended depending on the penetration of the probe itself. Of course, using an exponential window results are smoother and give us the attenuation curves observed in Fig. 4 if reported in a logarithmic section. Finally, we show in Fig. 12 a schematic representation of the evolving

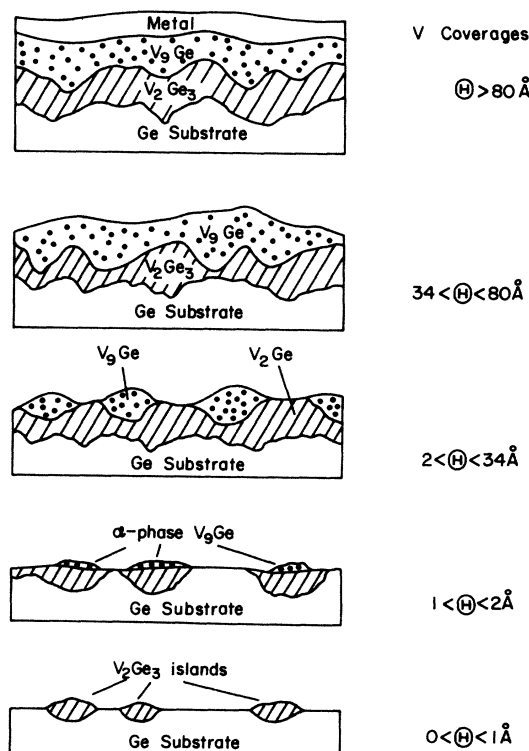


FIG. 12. Schematic representation of the V/Ge(111) interface evolution.

V/Ge(111) interface. According to our model, after a first region in which reacted islands of first-component phase are formed ( $0 < \Theta \leq 1$  Å), a two-phase region develops with the  $\alpha$  phase always growing on top of the first phase ( $1 \leq \Theta \leq 34$  Å). This competitive or two-phase growth mode ultimately ends up with the  $\alpha$  phase completely covering the reacted surface. At this point only phase 2 is formed. After  $\Theta = 80$  Å, a metal overlayer starts to develop, burying the reacted interface. This morphology is a consequence of reaction at the Ge surface, intermixing, the formation of a diffusion barrier, and the ultimate limitation in reaction imposed by diffusion.

#### Ce/Si(111)

The reactive behavior of Ce on Si is similar to that of V on Ge, but the room-temperature results show that the first reaction product is much more limited in coverage. As the results of Figs. 2 and 5 show, the experimental core line shapes can be decomposed into the substrate and two reacted phases and the growth attenuation of each can be followed. Using the formalism discussed above, we see that the first-phase reaction starts at 0.5 Å and that the second phase begins at 2 Å. As shown in the proposed phase diagram of Fig. 8, the two-phase region extends from 2 Å until  $\sim 9$  Å, with the second or final phase continuing to grow to the highest coverage studied (40 Å). At a photon energy of 135 eV, the photoelectron escape depths are 5 Å through the substrate and the first reacted phase and about 6 Å through the second phase. The best fit for the Si/Ce compositions are  $0.55 \pm 0.05$  and  $0.08 \pm 0.05$ . As discussed in Appendix B, the uncertainties in the compositions arise from the error bars for each experimental point in the growth-attenuation curves. They can therefore be reduced as the quality of the data themselves improves. As for V/Ge, the second phase is most likely a saturated solution of Si in polycrystalline Ce.

In a previous paper on the formation of the Ce/Si interface we had reached qualitatively similar conclusions for interface growth.<sup>7</sup> At ultralow coverages ( $\Theta \leq 0.6$  ML = 1.5 Å), we showed that clusters formed and that these clusters disrupted spontaneously to form the silicide.<sup>13</sup> Given our error bars on the predicted onset coverages,  $\pm 1$  Å, we see that the present conclusions are not inconsistent with the cluster-induced-reaction interpretation.

As for the V/Ge interface, we find that modeling allows us to predict onset and completion coverages with a high level of accuracy. Significantly, we see that for the Ce/Si system the values for the important coverages are much lower than those for V/Ge. We can see, for example, that the second phase (the dilute phase) appears at  $\sim 2$  Å rather than  $\sim 18$  Å and that the first phase ceases to form after  $\sim 9$  Å rather than  $\sim 34$  Å. This allows us to confirm that the V/Ge interface is far more extended—and that out diffusion of Ge is much greater than Si in the respective reacted regions. Such information is clearly important in applications where intermixing is to be minimized. We conclude that the chemical trapping via compound formation is stronger in the more reactive Ce/Si interface.

#### Ce/Ge(111)

The interface framed between Ce and Ge(111) is more complicated than those discussed above because there are three reacted core lines, as shown in Fig. 3. This raises the issue of partitioning of the three components. It can easily be shown that there is no unique solution and that partitioning can be obtained only by introducing at least a quadratic correction to the linear lever rule. Our calculations show that this kind of correction modifies the shape of the first-phase growth-attenuation curve, but does not affect the maximum value, i.e., the calculated atomic fraction is quite independent of the extension of the lever rule to a system of three coexisting phases of two components. For the sake of simplicity, we have modeled the three-phase region ( $2 \leq \Theta \leq 8$  Å) using the two-phase lever rule between the first and the second reacted species, neglecting the third one. This approximation is justified if, as in our case, the third component has such a low intensity that it does not play a relevant role in determining the maximum value for the growth-attenuation curve of the first species. Nevertheless, the shape and consequently the fit of the first-component growth-attenuation curve can be substantially modified by this approximation. After 8 Å, the system is reduced to two phases and partitioning is again straightforward.

Comparison of the dashed-line fits shown in Fig. 6 with the experimental results shows excellent agreement. In this case the first reacted component appears immediately upon deposition of Ce onto the surface. The second reacted component appears at 2 Å and the two-phase region continues until the onset of the most dilute phase at 3 Å. Completion of phase one occurs at 8 Å, phase two at 19 Å, and the final phase at 50 Å. Unfortunately, the available data extend to only 30 Å, and we cannot prove this last point. Nevertheless, the agreement of experiment and the model makes it possible to predict this cutoff with a reasonably high level of confidence. It is just the confidence which we seek for other systems.

The values of the Ge atomic concentration which provided the best fit were  $0.90 \pm 0.05$  for the first phase,  $0.40 \pm 0.05$  for the second phase, and  $0.11 \pm 0.05$  for the final phase. This indicates that the first region in the proposed phase diagram of Fig. 8(d) is associated with the solid solution of Ce in Ge and the composition that we obtain is the terminal solubility limit. After 2 Å a new compound forms that ranges between CeGe<sub>2</sub> and CeGe. At higher coverage another  $\alpha$  phase appears which corresponds to Ge dissolved in the Ce matrix. The complete evolution of the interface can then be described in terms of regions in which the different species vary in relative amounts. It is interesting to note that in this system we were able to detect both kinds of  $\alpha$  phases (metal-rich and semiconductor-rich) because of the very high experimental resolution possible for Ge 3d core studies and the relatively low capability of Ce to cover the substrate (1 ML = 2.7 Å).

#### INFLUENCE OF MORPHOLOGY ON THE VALIDITY OF THE MODEL

Several kinds of growth modes involving different morphologies have been proposed for metal-semiconductor in-

terfaces because the goal has been to determine the possible configurations for metal atoms on the surface.<sup>5,29</sup> For unreactive interfaces, this has been a challenging task, but it becomes much more difficult for reactive ones where disruption and continuous removal of substrate atoms occurs at the interface. This is, of course, one of the main difficulties in mathematically modeling the evolution of the reaction.

#### Island formation

In the course of our modeling of the experimental results, we examined several growth morphologies based on laminar structures and island formation. Significantly, attempts in determining a morphology which could describe the evolution of the interfaces over a wide range of coverages (0–100 Å) were largely unsuccessful, as described below for cylindrical clusters.

One of the morphological modes that we investigated was a cluster model of the kind reported by Ludeke and others<sup>29</sup> for Ag/GaAs. If we assume cylindrical clusters of reacted species of base area  $a$  and height  $l$ , the fraction of the surface covered is  $A = n_c a = n_c \pi R^2$ , where  $n_c$  is the cluster density per  $\text{cm}^{-2}$  and  $R$  is the radius of the clusters. The volume occupied by the clusters per  $\text{cm}^2$  will be  $Al$ , assuming that islands of the same size are formed. With this assumption, the normalized emission from the substrate will be

$$\frac{I_s}{I_s(0)} = 1 + A(e^{-l/\lambda_i} - 1),$$

where  $\lambda_i$  is the photoelectron escape depth through the reacted and clustered species. Similar results are obtained

$$\frac{I_s}{I_s(0)} = 1 + n_c \pi \left[ \frac{l_m v_a}{n_c \pi \alpha} \left( \frac{x+y}{x} \right) \right]^{2/3} \Theta^{2/3} \left[ \exp \left\{ - \left[ \frac{l_m \Theta v_a}{n_c \pi \alpha} \left( \frac{x+y}{x} \right) \right]^{1/3} \frac{\alpha}{\lambda_1} \right\} - 1 \right]$$

and

$$\frac{I_1}{I_s(0)} = C_1 \frac{\lambda_1}{\lambda_0} n_c \pi \left[ \frac{l_m v_a}{n_c \pi \alpha} \left( \frac{x+y}{x} \right) \right]^{2/3} \Theta^{2/3} \left[ 1 - \exp \left\{ - \left[ \frac{l_m \Theta v_a}{n_c \pi \alpha} \left( \frac{x+y}{x} \right) \right]^{1/3} \frac{\alpha}{\lambda_1} \right\} \right].$$

These equations are very sensitive to variations in the aspect ratio  $\alpha$  and the cluster density  $n_c$ . Intuitively, we must expect that as  $n_c$  increases, the effect of clustering will decrease (in the limit,  $n_c$  will equal the number of atoms deposited and the system will converge to laminar growth). Likewise, if  $\alpha$  increases to give tall, thin cylinders, the attenuation will increasingly diverge from exponential attenuation. Indeed, for  $l > \lambda$ , the substrate decays as

$$\frac{I_s}{I_s(0)} = 1 - n_c \pi \left[ \frac{l_m v_a}{n_c \pi \alpha} \left( \frac{x+y}{x} \right) \right]^{2/3} \Theta^{2/3}.$$

From this analysis, we conclude the following. First, a typical signature for cluster formation is a slower-than-laminar attenuation until the islands coalesce, as discussed previously by Ludeke.<sup>29</sup> After the coalescing point, it can decay exponentially (laminar growth) or new islands can

using hemispherical islands. Normalized emission from the first reacted species assumes the form

$$\frac{I_1}{I_s(0)} = AC_1 \frac{\lambda_1}{\lambda_0} [1 - e^{-l/\lambda_1}].$$

Then, if  $l$  is the thickness of the reacted region following the deposition of adatoms which form a compound through the reaction  $xM + yS = M_x S_y$ , we can write

$$n_m = \rho_m \Theta$$

and

$$n_s = \frac{n_m}{x} y$$

per unit area where  $\rho$  is the density of the metal, and  $n_m$  and  $n_s$  are the numbers of evaporated metal and reacted semiconductor atoms, respectively. Assuming an atomic average volume  $v_a$  for each atom, we have

$$V = n_c \pi R^2 l = (n_m + n_s) v_a = l_m \Theta \left[ \frac{x+y}{x} \right] v_a.$$

If we assume that the clusters have a fixed aspect ratio such that  $\alpha = l/R$ , we obtain

$$V = n_c \pi R^3 \alpha = l_m \Theta \left[ \frac{x+y}{x} \right] v_a$$

and

$$R = \left[ \frac{l_m \Theta}{n_c \pi \alpha} \left[ \frac{x+y}{x} \right] v_a \right]^{1/3}.$$

Our growth and attenuation curve then becomes

form on the reacted overlayer (Stranski-Krastinov mode). During this growth, there is little dependence of the substrate attenuation on  $h\nu$ . This is in contrast to what we have observed, since our results for V/Ge(111) follow an exponential attenuation (not an  $S$ -shaped curve) even if the substrate curves are almost  $h\nu$  independent.

#### CONCLUDING REMARKS

The method presented here is microscopic enough to determine heterogeneities at metal-semiconductor interfaces, but we cannot say whether these heterogeneities are related to single-species structure formation (large grains or crystallites) or if the intermixing between reacted species is on a much smaller scale. Although important for detailed microstructural analysis, this information is less important for our modeling once it is possible to describe these systems in terms of bulk thermodynamics,

averaging the heterogeneity across the sample surface. Indeed, when the overlayer coverage reaches a few monolayers, the interface is heterogeneous with two or three different phases that are not depleting each other. As the total number of semiconductor atoms available at any given location diminishes with increasing coverage, the metal-rich reaction products are favored and their relative concentration increases. The decomposition of the total attenuation curves of Figs. 4–6 into single-component growth-attenuation curves gives a picture of the reacted film in terms of relative concentration when the appropriate overlayer transmission properties are included [Eq. (6)].

We suggest that our model is of general validity and that it leads to extremely detailed descriptions of each system. The approximate values for the concentrations reported here have an error which is essentially due to the accuracy of the experimental results, as discussed in Appendix B, and they can be improved. As this is done, it will be possible to directly compare the interface phase diagrams to those of the bulk which are for equilibrium configurations.<sup>21</sup>

The extension of modeling to metal overlayers on compound semiconductor interfaces is presently underway. We have examined the Ce/GaAs (Ref. 15) and Sm/GaAs (Ref. 16) interfaces and the results show the presence of reacted species with well-defined metal-As stoichiometries. In contrast, the Ga 3*d* core shifts steadily with increasing metal coverage and this has been interpreted as indicating a continuous change in the Ga environment (diffusion in the metal matrix and progressive dilution). The chemistry involved in this interface is, however, more complex and several possible chemical reactions must be tested. The results presented here represent a first step. Future work must examine the effects of variations in temperature and must push for even higher resolution.

$$\frac{I_1}{I_{s0}} = C_1 \left( \frac{\lambda_1}{\lambda_0} \right) \left[ 1 - \exp \left[ - \frac{\Theta}{\lambda_1} \right] \right] \left\{ \left[ 1 - \left( \frac{\Theta - \Theta_2}{\Theta_1^* - \Theta_2} \right) \right] + \left[ \frac{\Theta - \Theta_2}{\Theta_1^* - \Theta_2} \right] \exp \left[ - \frac{\Theta - \Theta_2}{\lambda_2} \right] \right\}. \quad (\text{A2})$$

This description is valid until the variation of the signal due to the growth of the first phase is so small relative to the attenuation effect of the second species that only the second can be resolved experimentally. This is expressed by the condition

$$\frac{d \ln \left( \frac{I_1}{I_0} \right)}{d\Theta} = - \frac{1}{\lambda_2}, \quad (\text{A3})$$

which defines the value  $\Theta = \Theta_D$ . At higher coverages, we assume that the first species is simply covered up by the second one. If  $\Theta_D < \Theta_1^*$ , Eq. (A2) becomes

$$\frac{I_1}{I_{s0}} = C_1 \left( \frac{\lambda_1}{\lambda_0} \right) \left[ 1 - \exp \left[ - \frac{\Theta_D}{\lambda_1} \right] \right] \times \left[ \exp \left[ - \frac{(\Theta - \Theta_D)}{\lambda_2} \right] \right] F, \quad (\text{A4})$$

We anticipate that such studies will lead to predictive capabilities for interfaces.

#### ACKNOWLEDGMENTS

Stimulating discussions with R. Ludeke, J. L. Freeouf, S. A. Chambers, M. W. Ruckman, M. Grioni, and J. J. Joyce are gratefully acknowledged. This work was supported by U.S. Office of Naval Research (ONR) under Contract No. N00014-83-K-0579.

#### APPENDIX A: MATHEMATICAL DERIVATIONS

To model photoelectron propagation through a composite region, we adopt the following definitions:  $C_i$  is the atomic fraction of the semiconductor atoms in phase  $i$ ;  $\lambda_i$  is the intrinsic electron mean free path in phase  $i$ ;  $I_s(0)$  is the intensity of the semiconductor core emission of the pure substrate;  $I_i/I_s(0)$  is the intensity of the semiconductor core emission originating from semiconductor atoms in phase  $i$  normalized to the emission from the clean substrate;  $\Theta_i$  is the onset coverage for the formation of species  $i$ ; and  $\Theta_i^*$  is the end coverage for species  $i$ . In the following we refer to a two-phase region where the first phase grows directly in contact with the substrate and the second phase is formed only subsequently, giving rise to an intermixed two-phase region.

(1) Phase 1 shows that for  $\Theta < \Theta_1$  the only species that forms is characterized by the subscript 1. In this region, we have a simple growth curve expressed by

$$\frac{I_1}{I_s(0)} = C_1 \left( \frac{\lambda_1}{\lambda_0} \right) \left[ 1 - \exp \left[ - \frac{\Theta}{\lambda_1} \right] \right]. \quad (\text{A1})$$

The second phase starts to form after  $\Theta_2$ , and partitioning through the lever rule is necessary. We then have

where

$$F = \left\{ \left[ \frac{\Theta_D - \Theta_2}{\Theta_1 - \Theta_2} \right] \exp \left[ - \frac{(\Theta_D - \Theta_2)}{\lambda_2} \right] + \left[ 1 - \left[ \frac{\Theta_D - \Theta_2}{\Theta_1 - \Theta_2} \right] \right] \right\}.$$

After this point, the first phase is covered up and transmission through the overlayer is characterized by  $\lambda_2$ , the escape depth of the second phase. On the other hand, if  $\Theta_D > \Theta_1^*$ , then after  $\Theta_1^*$  Eq. (A2) becomes

$$\frac{I_1}{I_{s0}} = C_1 \left( \frac{\lambda_1}{\lambda_0} \right) \left[ 1 - \exp \left[ - \frac{\Theta_1^*}{\lambda_1} \right] \right] \exp \left[ \frac{\Theta - \Theta_2}{\lambda_2} \right], \quad (\text{A5})$$

where

$$[(\Theta - \Theta_2)/(\Theta_1^* - \Theta_2)]_{\Theta = \Theta_1^*} = 1$$

and the condition of exponential decay is satisfied.

(2) Phase 2 starts to form for  $\Theta > \Theta_2$  but at a rate slower by a factor  $(\Theta - \Theta_2)/(\Theta_1^* - \Theta_2)$ . Then

$$\frac{I_2}{I_{s0}} = \left[ \frac{\Theta - \Theta_2}{\Theta_1^* - \Theta_2} \right] C_2 \left[ \frac{\lambda_2}{\lambda_0} \right] \left[ 1 - \exp \left[ - \frac{(\Theta - \Theta_2)}{\lambda_2} \right] \right]. \quad (\text{A6})$$

This is true until the first phase is completed ( $\Theta = \Theta_1^*$ ). Afterward,

$$\frac{I_2}{I_{s0}} = C_2 \left[ \frac{\lambda_2}{\lambda_0} \right] \left[ 1 - \exp \left[ - \frac{(\Theta - \Theta_2)}{\lambda_2} \right] \right]. \quad (\text{A7})$$

This expression saturates at  $C_2(\lambda_2/\lambda_0)$  unless another phase starts to form or metal covers it up. In that case,

$$\frac{I_2}{I_{s0}} = C_2 \left[ \frac{\lambda_2}{\lambda_0} \right] \left[ 1 - \exp \left[ - \frac{(\Theta - \Theta_2)}{\lambda_2} \right] \right] \left\{ \left[ 1 - \frac{\Theta - \Theta_3}{\Theta_2^* - \Theta_3} \right] + \left[ \frac{\Theta - \Theta_3}{\Theta_2^* - \Theta_3} \right] \exp \left[ - \frac{(\Theta - \Theta_3)}{\lambda_3} \right] \right\}. \quad (\text{A8})$$

## APPENDIX B: FITTING PARAMETERS

In the following we describe the sensitivity of Eq. (8) to variations in the fitting parameters. To do this, we show in Fig. 13 the experimental points for the first reacted phase for V/Ge(111) as obtained from the core-level decomposition and show representative fittings. Anal-

gous plots can be obtained for other components and for different interfaces.

When two reacted species are simultaneously present, we can define a two-phase region using the parameters  $\Theta_2$  and  $\Theta_1^*$ . In this region, the reaction is controlled by out diffusion of Ge through the reacted overlayer. Setting these two parameters means defining the region where the maximum for the single-species growth attenuation curve must be. This position is insensitive to small variations in  $\Theta_2$  and  $\Theta_1^*$  but depends on the width of the interval chosen. At the same time, variations in those two parameters shift the growth and attenuation part of the curve leaving almost invariant the absolute value of the "plateau" region. This is shown in Figs. 13(a) and 13(b) where small variations ( $\pm 1$  Å) affect the decay-curve starting point. It is then possible by increasing one value and decreasing the other to produce a good fit of the initial and final slopes of the curve. In Fig. 13(c) we show that the turning point is strongly dependent on the value of the concentration  $C_1$  chosen. Indeed, small variations ( $\Delta C_i = \pm 0.05$ ) are able to move the maximum of the curve through the scatter of the experimental points. At this point, we see that the uncertainty in the numbers proposed for the parameters is due to the experimental scatter in the results. More precise and more numerous data are therefore necessary for better quantitative modeling. This is even more evident when studying a metal-rich phase since small variations  $\Delta C_i = \pm 0.01$  are enough to produce significant modifications in the single-component curve, but the experimental error does not allow sufficiently high accuracy to determine  $C_i$  to better than  $\pm 0.05$ .

Finally, in Fig. 13(d) we show a set of curves for combined parameter variations which indicates that the best fit is obtained for  $C_i = 0.60$ ,  $\Theta_2 = 1$  Å, and  $\Theta_1^* = 34$  Å. The accord between results and calculation is impressive. Moreover, we note that the parameters determined by the fit of one phase must remain invariant in fitting the remaining phases. These are also affected by the first-phase parameter determinations, as shown in Eq. (A2) in Appendix A. This coupling between the growth-attenuation curves for different phases is a requirement for maintaining self-consistency for the curves at all photon energies since these parameters are independent of  $h\nu$ .

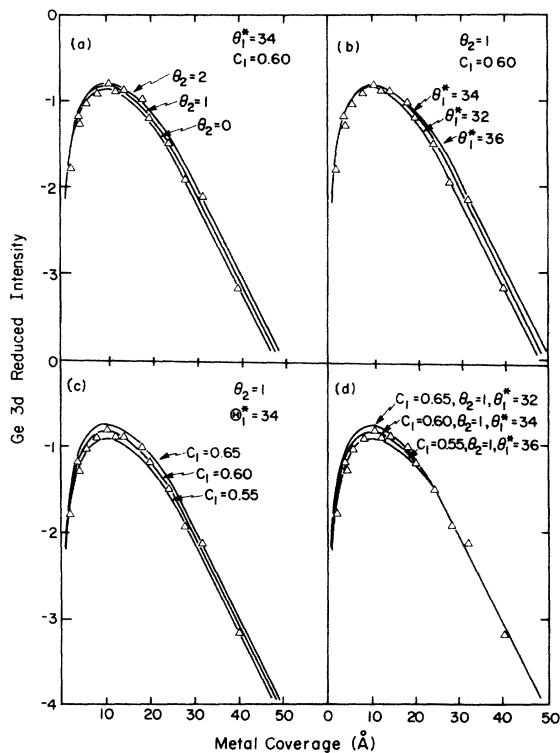


FIG. 13. Plot of Eq. (8) for different values of the parameters used in our modeling of the experimental results for V/Ge(111). As shown, variations in the coverages shift the calculated results laterally, whereas variations in concentration for the reacted species shift the calculated results vertically. The best fit is obtained iteratively, as shown in (d).

- \*Permanent address: Department of Chemistry, University of Pittsburgh, Pittsburgh, PA 15260.
- <sup>1</sup>L. J. Brillson, *Surf. Sci. Rep.* **2**, 123 (1982); J. H. Weaver, in *Analysis and Characterization of Thin Films*, edited by K. N. Tu and R. Rosenberg (Academic, New York, in press).
  - <sup>2</sup>G. Le Lay, *Surf. Sci.* **132**, 169 (1983).
  - <sup>3</sup>G. Rossi, I. Abbati, L. Braicovich, I. Lindau, and W. E. Spicer, *J. Vac. Sci. Technol.* **21**, 617 (1982).
  - <sup>4</sup>J. R. Waldrop, S. P. Kowalczyk, and R. W. Grant, *J. Vac. Sci. Technol.* **21**, 607 (1982).
  - <sup>5</sup>A. Franciosi, D. J. Peterman, J. H. Weaver, and V. L. Moruzzi, *Phys. Rev. B* **25**, 4981 (1982).
  - <sup>6</sup>L. J. Brillson, C. F. Brucker, G. Margaritondo, J. Slovek, and N. G. Stoffel, Proceedings of the 15th International Conference on the Physics of Semiconductors, Kyoto, 1980 [*J. Phys. Soc. Jpn.* **59**, 1089 (1980)].
  - <sup>7</sup>M. Grioni, J. J. Joyce, M. del Giudice, D. G. O'Neill, and J. H. Weaver, *Phys. Rev. B* **20**, 7370 (1984).
  - <sup>8</sup>A. Zunger, *Phys. Rev. B* **24**, 4372 (1981).
  - <sup>9</sup>R. R. Daniels, A. D. Katnani, Te-Xiu Zhao, G. Margaritondo, and Z. Zunger, *Phys. Rev. Lett.* **49**, 895 (1982).
  - <sup>10</sup>G. Margaritondo, J. E. Rowe, and S. B. Christman, *Phys. Rev. B* **14**, 5396 (1976).
  - <sup>11</sup>W. E. Spicer, I. Lindau, P. Skeath, C. Y. Su, and P. Chye, *Phys. Rev. Lett.* **44**, 420 (1980); G. W. Rubloff, *Surf. Sci.* **132**, 268 (1983).
  - <sup>12</sup>M. del Giudice, J. J. Joyce, M. W. Ruckman, and J. H. Weaver, *Phys. Rev. B* **32**, 5149 (1985).
  - <sup>13</sup>M. Grioni, J. J. Joyce, S. A. Chambers, D. G. O'Neill, M. del Giudice, and J. H. Weaver, *Phys. Rev. Lett.* **53**, 2331 (1984); see also M. Grioni, J. J. Joyce, M. del Giudice, D. G. O'Neill, and J. H. Weaver, *Phys. Rev. B* **20**, 7370 (1984).
  - <sup>14</sup>M. del Giudice, M. Grioni, J. J. Joyce, M. W. Ruckman, S. A. Chambers, and J. H. Weaver, *Surf. Sci.* (to be published); M. Grioni, M. del Giudice, J. J. Joyce, and J. H. Weaver, *J. Vac. Sci. Technol. A* **3**, 907 (1985).
  - <sup>15</sup>J. H. Weaver, M. Grioni, J. J. Joyce, and M. del Giudice, *Phys. Rev. B* **31**, 5290 (1985) (Ce/GaAs).
  - <sup>16</sup>J. H. Weaver, M. Grioni, and J. J. Joyce, *Phys. Rev. B* **31**, 5348 (1985) for Cr/GaAs; M. Grioni, J. J. Joyce, and J. H. Weaver, *J. Vac. Sci. Technol. A* **3**, 918 (1985) for V/GaAs; M. W. Ruckman, M. del Giudice, J. J. Joyce, and J. H. Weaver, *Phys. Rev. B* **33**, 2191 (1985) for Ti/GaAs.
  - <sup>17</sup>L. Darken and R. Gurry, *Physical Chemistry of Metals* (McGraw-Hill, New York, 1953) (Chapter 13 contains a description of heterogeneous equilibria and the lever rule for two coexisting phases).
  - <sup>18</sup>M. del Giudice, R. A. Butera, M. W. Ruckman, J. J. Joyce, and J. H. Weaver, *J. Vac. Sci. Technol.* (to be published) presents a temperature-dependent study of the V/Ge(111) interface.
  - <sup>19</sup>F. J. Grunthaner (private communication) has taken a mean-free-path variation into account for interfaces involving oxide formation.
  - <sup>20</sup>See, for example, the discussion of surface segregation by Brillson in Ref. 1 above.
  - <sup>21</sup>Although there is the temptation to relate the interface results to the "normal phase diagram," it would be surprising if the phase diagram for the interface were identical to the bulk because the thermodynamic conditions differ. Unfortunately, little is known about the details of these differences.
  - <sup>22</sup>M. Grioni, J. J. Joyce, and J. H. Weaver, *Phys. Rev. B* **32**, 926 (1985) for Sm/GaAs.
  - <sup>23</sup>D. E. Eastman, T.-C. Chiang, P. Heimann, and F. J. Himpsel, *Phys. Rev. Lett.* **45**, 656 (1980); F. J. Himpsel, P. Heimann, T.-C. Chiang, and D. E. Eastman, *ibid.* **45**, 1112 (1980); S. Brennan, J. Stöhr, R. Jaeger, and J. E. Rowe, *ibid.* **45**, 1414 (1980).
  - <sup>24</sup>G. Rossi, I. Lindau, L. Braicovich, and I. Abbati, *Phys. Rev. B* **28**, 3031 (1983).
  - <sup>25</sup>A. Franciosi, D. J. Peterman, and J. H. Weaver, *J. Vac. Sci. Technol.* **19**, 657 (1981); see also L. J. Brillson, *Surf. Sci. Rep.* **2**, 123 (1982); J. H. Weaver, in *Analysis and Characterization of Thin Films*, edited by K. N. Tu and R. Rosenberg (Academic, New York, in press).
  - <sup>26</sup>Until now, we have had no way of assessing the variation of  $\lambda_i$  for a reacting interface, although it has been reasonable to expect changes when the plasma frequencies vary.
  - <sup>27</sup>M. P. Seah and W. A. Dench, *Surf. Interface Anal.* **1**, 2 (1979).
  - <sup>28</sup>G. N. Lewis and M. Randall, *Thermodynamics*, 2nd ed. (McGraw-Hill, New York, 1961).
  - <sup>29</sup>R. Ludeke, *Surf. Sci.* **132**, 169 (1983); R. Ludeke, T.-C. Chiang, and T. Miller, *J. Vac. Sci. Technol. B* **1**, 581 (1983).